TSINGHUA SCIENCE AND TECHNOLOGY
ISSN 1007-0214 08/10 pp728–737
DOI: 10.26599/TST.2018.9010102
Volume 24, Number 6, December 2019

Anchor Self-Localization Algorithm Based on UWB Ranging and Inertial Measurements

Qin Shi, Sihao Zhao, Xiaowei Cui*, Mingquan Lu, and Mengdi Jia

Abstract: Localization systems utilizing Ultra-WideBand (UWB) have been widely used in dense urban and indoor environments. A moving UWB tag can be located by ranging to fixed UWB anchors whose positions are surveyed in advance. However, manually surveying the anchors is typically a dull and time-consuming process and prone to artificial errors. In this paper, we present an accurate and easy-to-use method for UWB anchor self-localization, using the UWB ranging measurements and readings from a low-cost Inertial Measurement Unit (IMU). The locations of the anchors are automatically estimated by freely moving the tag in the environment. The method is inspired by the Simultaneous Localization And Mapping (SLAM) technique used by the robotics community. A tightly-coupled Error-State Kalman Filter (ESKF) is utilized to fuse UWB and inertial measurements, producing UWB anchor position estimates and six Degrees of Freedom (6DoF) tag pose estimates. Simulated experiments demonstrate that our proposed method enables accurate self-localization for UWB anchors and smooth tracking of the tag.

Key words: anchor self-localization; error-state Kalman filter; sensor fusion; simultaneous localization and mapping

1 Introduction

Indoor location awareness is key to a number of applications. Many indoor localization technologies have been developed in recent years for research and commercialization[1]. Among these technologies, the relatively new Ultra-WideBand (UWB) method has gained extensive attention due to its high-ranging accuracy[2]. Short-pulse radio waveforms are utilized in UWB, leading to an accurate determination of transceiving timestamps of the UWB signal between a transmitter and a corresponding receiver. Emerging applications of UWB localization systems have been presented in Refs. [3–7]. In a typical localization scenario using the UWB characteristic, a transmitter (namely a tag) is to be located, and several receivers (namely anchors) are rigidly fixed at static known locations receiving the radio wave signals. The location of the tag can then be obtained by processing measurements such as Time Of Flight (TOF)[4], Time Of Arrival (TOA)[8], Time Difference Of Arrival (TDOA)[9,10], etc.[1] A UWB localization accuracy to the order of decimeters is achieved[11].

However, in UWB localization systems, the position of the UWB anchors is assumed to be pre-calibrated and known. Pre-calibration by manually surveying the anchors is always a part of the deployment of an UWB localization system. Nevertheless, surveying the anchors requires additional equipment, such as a laser rangefinder, and is typically a grueling, time-consuming process that is prone to artificial errors. Furthermore, the pre-calibration process cannot be conducted in areas unreachable or dangerous for mankind, such as narrow spaces or high-radiation areas. Therefore, an anchor self-localization method is desirable to automate the process that determines the physical location of the anchors, thus reducing time and labor costs.

For UWB systems, the direct ranges from anchors

• Qin Shi, Sihao Zhao, Xiaowei Cui, Mingquan Lu, and Mengdi Jia are with the Department of Electronic Engineering, Tsinghua University, Beijing 100084, China. E-mail: cxw2005@mail.tsinghua.edu.cn.
* To whom correspondence should be addressed.
Manuscript received: 2018-04-16; revised: 2018-04-24; accepted: 2018-04-25

to a tag can be measured. By setting the tag at known positions, the anchor self-localization problem becomes an inverted localization problem and the positions of the anchors can be determined by solving multilateration equations. However, this still presents challenges for unreachable or dangerous areas when setting the tag. Additionally, obtaining the tag positions is typically a chicken and egg problem, as the UWB localization system is not available. Inspired by the cooperative sensor localization algorithms in Wireless Sensor Networks (WSN)[12], the UWB anchor self-localization problem can be addressed with the underlying assumption that communication between UWB anchor pairs is available. However, this significantly complicates the UWB transmission scheme design and raises power costs.

An accurate anchor self-localization solution was presented in Ref. [13]. Firstly, a tag at the known location was rigidly attached to each anchor, thus obtaining its pairwise relative position as a constraint to a maximum-likelihood optimization problem. Gaussian noise modeled TOA measurements were utilized in formulating this optimization problem, the solution to which allowed for the estimation of the initial anchor positions. Secondly, a data set was collected by freely moving a single tag in the measurement volume, and the initial position estimations of the tag were optimized using the previous estimated initial anchor positions. Finally, a complete parameter vector, including the tag and the anchor positions, was estimated on the same data set. This optimization began from the initial estimation results derived in the first two steps. To handle the UWB measurement outliers, this calibration solution was enhanced in Ref. [14] by modeling the UWB measurements using heavy-tailed asymmetric distribution. However, due to the nature of UWB, the calibration accuracy of this solution degrades in multipath propagation and Non-Line-Of-Sight (NLOS) situations. Further, the initialization steps are complicated, considering the numbers of tags that need to be attached and detached.

In this paper, we present an accurate and easy-to-use UWB anchor self-localization method by introducing an additional low-cost Inertial Measurement Unit (IMU) consisting of a 3-axis rate gyroscope and a 3-axis accelerometer. By additionally attaching an IMU to the tag, an accurate position estimate can be obtained in a short period of time after system startup, which we use as a constraint to derive a reliable initial estimate of the anchor positions. Furthermore, the IMU measurements are incorporated into the UWB self-localization algorithm as constraints and are capable of improving system robustness in signal multipath and NLOS situations. The anchor self-localization method is based on the tightly coupled fusion of the raw IMU measurements and UWB ranging measurements, which permits simultaneous localization of the tag and self-localization of the anchors. We do not require a known displacement trajectory of the tag or any related action to obtain a priori, but instead let the tag move freely in the environment, thereby enabling an automatic deployment of a UWB localization system.

In the remainder of this paper, we first give a detailed formulation of our UWB anchor self-localization problem in Section 2, followed by the formulation of the sensor models in Section 3. We then solve the UWB anchor self-localization problem using UWB and inertial measurements in Section 4. Finally, we provide the experimental results and conclusion in Sections 5 and 6, respectively.

2 Problem Formulation

In this section, we will address the UWB anchor self-localization problem with a detailed formulation. We start by introducing a typical application.

Considering localization for construction teams in underground construction tasks, UWB anchors embedded in mobile stands can be incrementally placed as the construction areas become larger. It is convenient to use the anchor self-localization method for a quick and accurate determination of the current anchor positions, by freely moving an IMU mounted UWB tag in the new construction area. Figure 1 illustrates this

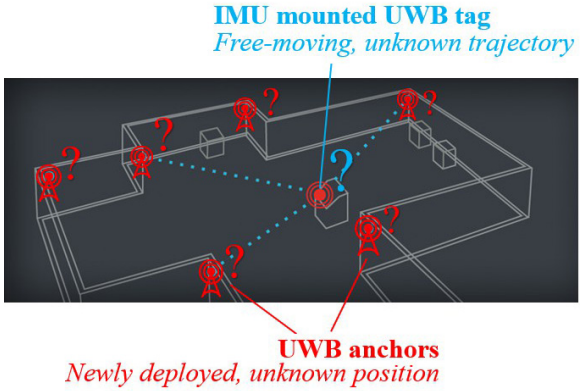

Fig. 1 A typical anchor self-localization scenario: when UWB anchors are newly deployed, they are self-localized by freely moving an IMU mounted UWB tag in the measurement volume.

typical application scenario. Here we note that the IMU is rigidly connected to the UWB tag with known relative positions. This setup shares a common clock, which enables timestamped UWB and inertial measurements and thus simplifies processing.

Several coordinate frames are introduced: the body frame which is fixed with the IMU sensor is denoted as $(\cdot)^b$, the tangent frame whose origin is fixed on the earth is denoted as $(\cdot)^t$, the Earth-Centered Inertial (ECI) frame is an inertial frame denoted as $(\cdot)^i$, and the Earth-Centered Earth-fixed Frame (ECEF) is denoted as $(\cdot)^e$. In this work, the tangent frame is selected as the reference computational frame. Notations that are employed throughout the work are as follows. The three-dimensional vector $\boldsymbol{r}$ expressed in a reference frame k is written as $\boldsymbol{r}^k$ or alternatively as $\boldsymbol{r}^k_{AB}$, with A and B as start and end points, respectively. The instantaneous angular velocity of frame j with respect to frame i expressed in a reference frame k is written as $\boldsymbol{\omega}^k_{ij}$. $\boldsymbol{R}^k_i$ is the rotation matrix, representing rotation from frame i to frame k. The corresponding quaternion is written as $\boldsymbol{q}^k_i$ in S^3, which relates a 3-sphere S^3 to rotations of $\mathbb{R}^3$. A comprehensive overview of rotation representation is given in Ref. [15]. The matrix $[\boldsymbol{\omega}]^\times$ represents the skew symmetric form of vector $\boldsymbol{\omega}$.

The aim of our work is to develop a self-localization method that estimates the positions of the anchors expressed in the tangent frame:

$$\boldsymbol{x}_U := \begin{bmatrix} \boldsymbol{p}_1^{\mathrm{T}} & \cdots & \boldsymbol{p}_M^{\mathrm{T}} \end{bmatrix}^{\mathrm{T}} \in \mathbb{R}^{3M} \tag{1}$$

where $\boldsymbol{p}_1, \ldots, \boldsymbol{p}_M$ are the corresponding positions of anchors $a_1, \ldots, a_M$, M is the total number of anchors. The dimension of the state to be estimated is then $3M$. We have omitted the superscript t of position and velocity for simple representation in this paper.

Considering that we have no predetermined knowledge of the tag position, the self-localization problem becomes a Simultaneous Localization And Mapping (SLAM) problem, which has been widely researched in the robotics community[16–19]. SLAM is the algorithm by which a robot can simultaneously build a consistent map of the environment and estimate its location within this same map. A seminal solution to the SLAM problem utilizes an Extended Kalman Filter (EKF)[20,21]. Based on the idea of the SLAM scheme, the map in our self-localization problem refers to the positions of anchors. In this way, our self-localization algorithm aims to simultaneously recover the positions of all unknown anchors $\boldsymbol{x}_U$, and estimate the state of the tag (namely a robot) $\boldsymbol{x}_N$.

A variety of literature estimates the state of the tag using inertial and UWB measurements with UWB anchor positions known, in which case the state $\boldsymbol{x}_N$ is typically defined as Refs. [22–24]:

$$\boldsymbol{x}_N := \begin{bmatrix} \boldsymbol{p}^{t\,\mathrm{T}} & \boldsymbol{v}^{t\,\mathrm{T}} & \boldsymbol{q}_b^{t\,\mathrm{T}} \end{bmatrix}^{\mathrm{T}} \in \mathbb{R}^6 \times S^3 \tag{2}$$

where $\boldsymbol{p}^t$ is the position of the tag in the tangent frame, $\boldsymbol{v}^t$ is the tag velocity, the superscipt t indicates tag, $\boldsymbol{q}^t_b$ is the body orientation which is observable due to the benefit of IMU. In our work, following the above-mentioned literature, we additionally render the IMU biases observable and derive the state as

$$\boldsymbol{x}_N := \begin{bmatrix} \boldsymbol{p}^{t\,\mathrm{T}} & \boldsymbol{v}^{t\,\mathrm{T}} & \boldsymbol{q}_b^{t\,\mathrm{T}} & \boldsymbol{x}_a{}^{\mathrm{T}} & \boldsymbol{x}_g{}^{\mathrm{T}} \end{bmatrix}^{\mathrm{T}} \in \mathbb{R}^6 \times S^3 \times \mathbb{R}^6 \tag{3}$$

where $\boldsymbol{x}_a, \boldsymbol{x}_g$ are inertial biases explained in Section 3.1.

Thus, our goal is the estimation of the full state vector consisting of the positions of anchors $\boldsymbol{x}_U$ and the state of the tag $\boldsymbol{x}_N$:

$$\boldsymbol{x}_S := \begin{bmatrix} \boldsymbol{x}_N^{\mathrm{T}} & \boldsymbol{x}_U^{\mathrm{T}} \end{bmatrix}^{\mathrm{T}} \in \mathbb{R}^6 \times S^3 \times \mathbb{R}^{6+3M} \tag{4}$$

The raw IMU and UWB measurements are inputs into our method. Instead of the loosely-coupled method, in which the measurements are preprocessed as independent quantities like position or orientation, we advocate the direct use of the raw measurements for a tightly-coupled fusion. This permits maximal exploitation of sensing cues, thus leading to a robust system. For instance, when there are not enough UWB measurements to obtain a triangulation result in a loosely-coupled method, the UWB information will be ignored. A tightly-coupled method will directly use every raw measurement without information loss. Furthermore, the tightly-coupled method is capable of suppressing the outliers, especially the UWB measurement outliers that are due to multipath effects or NLOS situations. These benefits illustrate the motivation for adding an IMU as an aid.

Our fusion strategy relies on the Error-State Kalman Filter (ESKF)[25], which has been successfully used in estimation and data fusion problems. To derive the ESKF, we provide a detailed state model of the inertial and UWB sensors in the next section.

3 Sensor Modeling

In this section, we model the IMU and UWB measurements and formulate the error-state equations of the kinematics of the system.

3.1 IMU kinematics

IMU has been utilized as a valuable sensor in many applications. An IMU commonly measures the sensor's

specific force $\boldsymbol{f}^b$ and angular rate $\boldsymbol{\omega}_{ib}^b$ with respect to an inertial frame, such as an ECI frame, which is resolved in the body-fixed frame, using a 3-axis accelerometer and a 3-axis gyroscope. The sensor's specific force $\boldsymbol{f}^b$ is a combination of earth gravity field vector $\boldsymbol{g}_1^t$ and the sensor's acceleration $\boldsymbol{\alpha}_{tb}^t$:

$$\boldsymbol{f}^b = \boldsymbol{R}_t^b(\boldsymbol{\alpha}_{tb}^t - \boldsymbol{g}_1^t) \tag{5}$$

where $\boldsymbol{g}_1^t = \bar{\boldsymbol{g}}^t - \boldsymbol{\omega}_{ie}^t \times (\boldsymbol{\omega}_{ie}^t \times \boldsymbol{r})$, $\boldsymbol{\omega}_{ie}^t$ denotes the Earth's rotation vector with respect to the i-frame, $\boldsymbol{r}$ is the geocentric position vector, $\bar{\boldsymbol{g}}^t$ is the gravitational vector, and $\boldsymbol{\omega}_{ie}^t \times (\boldsymbol{\omega}_{ie}^t \times \boldsymbol{r})$ is the centripetal acceleration due to the Earth's rotation around its axis.

The raw measurements from the accelerometer and gyroscope, namely $\bar{\boldsymbol{\alpha}}$ and $\bar{\boldsymbol{\omega}}$:

$$\bar{\boldsymbol{\alpha}} = \boldsymbol{f}^b + \boldsymbol{x}_a + \boldsymbol{v}_a \tag{6}$$

$$\bar{\boldsymbol{\omega}} = \boldsymbol{\omega}_{ib}^b + \boldsymbol{x}_g + \boldsymbol{v}_g \tag{7}$$

where $\bar{\boldsymbol{\alpha}}$ and $\bar{\boldsymbol{\omega}}$ are affected by acceleration bias $\boldsymbol{x}_a$, gyroscope bias $\boldsymbol{x}_g$, and addictive noise. The addictive noise in acceleration and gyroscope measurements is assumed to be Gaussian white noise, $\boldsymbol{v}_a \sim \mathcal{N}(\boldsymbol{0}, \boldsymbol{\sigma}_{v_a}^2)$, $\boldsymbol{v}_g \sim \mathcal{N}(\boldsymbol{0}, \boldsymbol{\sigma}_{v_g}^2)$. The acceleration bias $\boldsymbol{x}_a$ is modeled as Brownian motion, whose derivative is first order Gauss-Markov process:

$$\dot{\boldsymbol{x}}_a = \boldsymbol{F}_a \boldsymbol{x}_a + \boldsymbol{\omega}_a \tag{8}$$

where $\boldsymbol{\omega}_a$ is the driving Gaussian white noise, $\boldsymbol{\omega}_a \sim \mathcal{N}(\boldsymbol{0}, \boldsymbol{\sigma}_{\boldsymbol{\omega}_a}^2)$. $\boldsymbol{F}_a$ corresponds to the correlation time of 3-axis acceleration bias:

$$\boldsymbol{F}_a = \begin{bmatrix} -\frac{1}{T_{ax}} & 0 & 0 \\ 0 & -\frac{1}{T_{ay}} & 0 \\ 0 & 0 & -\frac{1}{T_{az}} \end{bmatrix} \tag{9}$$

The gyroscope bias $\boldsymbol{x}_g$ is simply modeled as random walk, whose derivative is Gaussian white noise, $\boldsymbol{\omega}_g \sim \mathcal{N}(\boldsymbol{0}, \boldsymbol{\sigma}_{\boldsymbol{\omega}_g}^2)$.

$$\dot{\boldsymbol{x}}_g = \boldsymbol{\omega}_g \tag{10}$$

Therefore, we can write the IMU kinematics equations combined with dynamic bias models as

$$\begin{aligned} \dot{\boldsymbol{p}}^t &= \boldsymbol{v}^t, \\ \dot{\boldsymbol{v}}^t &= \boldsymbol{R}_b^t \boldsymbol{f}^b + \boldsymbol{g}^t - 2[\boldsymbol{\omega}_{ie}^t]^\times \boldsymbol{v}^t, \\ \dot{\boldsymbol{R}}_b^t &= \boldsymbol{R}_b^t([\boldsymbol{\omega}_{ib}^b]^\times - [\boldsymbol{\omega}_{ie}^b]^\times), \\ \dot{\boldsymbol{x}}_a &= \boldsymbol{F}_a \boldsymbol{x}_a + \boldsymbol{\omega}_a, \\ \dot{\boldsymbol{x}}_g &= \boldsymbol{\omega}_g \end{aligned} \tag{11}$$

To arrive at the error-state covariance propagation equation, we adapt the formulation from Ref. [26], in which the error term of the over-parameterized 9-dimensional rotation matrix is defined as a small perturbation around the estimated rotation matrix:

$$\boldsymbol{R}_b^t = (\boldsymbol{I_3} + [\boldsymbol{\rho}]^\times)\hat{\boldsymbol{R}}_b^t \tag{12}$$

where $\boldsymbol{\rho}$ is a 3-dimensional vector representing the small-angle rotations to rotate from the tangent frame to align with the estimated tangent frame with respect to the tangent frame and $\boldsymbol{I}_3$ is 3×3 identity matrix.

Therefore the error-state of the tag is derived:

$$\delta \boldsymbol{x}_N = \begin{bmatrix} \delta \boldsymbol{p}^{t\mathrm{T}} & \delta \boldsymbol{v}^{t\mathrm{T}} & \boldsymbol{\rho}^\mathrm{T} & \delta \boldsymbol{x}_a{}^\mathrm{T} & \delta \boldsymbol{x}_g{}^\mathrm{T} \end{bmatrix}^\mathrm{T} \in \mathbb{R}^{15} \tag{13}$$

The continuous-time linearized dynamics of error-state take the form as

$$\delta \dot{\boldsymbol{x}}_N(t) = \boldsymbol{F}(t)\delta \boldsymbol{x}_N(t) + \boldsymbol{G}(t)\boldsymbol{w}(t) \tag{14}$$

where $\boldsymbol{w} := \begin{bmatrix} \boldsymbol{v}_a^\mathrm{T} & \boldsymbol{v}_g^\mathrm{T} & \boldsymbol{\omega}_a^\mathrm{T} & \boldsymbol{\omega}_g^\mathrm{T} \end{bmatrix}^\mathrm{T}$ is the collection of uncorrelated Gaussian white noise processes, and

$$\boldsymbol{F} = \begin{bmatrix} \boldsymbol{0} & \boldsymbol{I}_3 & \boldsymbol{0} & \boldsymbol{0} & \boldsymbol{0} \\ \boldsymbol{0} & -2\left[\boldsymbol{\omega}_{ie}^t\right]^\times & -\left[\boldsymbol{f}^t\right]^\times & -\boldsymbol{R}_b^t & \boldsymbol{0} \\ \boldsymbol{0} & \boldsymbol{0} & -\left[\boldsymbol{\omega}_{ie}^t\right]^\times & \boldsymbol{0} & -\boldsymbol{R}_b^t \\ \boldsymbol{0} & \boldsymbol{0} & \boldsymbol{0} & \boldsymbol{F}_a & \boldsymbol{0} \\ \boldsymbol{0} & \boldsymbol{0} & \boldsymbol{0} & \boldsymbol{0} & \boldsymbol{0} \end{bmatrix} \tag{15}$$

$$\boldsymbol{G} = \begin{bmatrix} \boldsymbol{0} & \boldsymbol{0} & \boldsymbol{0} & \boldsymbol{0} \\ -\boldsymbol{R}_b^t & \boldsymbol{0} & \boldsymbol{0} & \boldsymbol{0} \\ \boldsymbol{0} & -\boldsymbol{R}_b^t & \boldsymbol{0} & \boldsymbol{0} \\ \boldsymbol{0} & \boldsymbol{0} & \boldsymbol{I}_3 & \boldsymbol{0} \\ \boldsymbol{0} & \boldsymbol{0} & \boldsymbol{0} & \boldsymbol{I}_3 \end{bmatrix} \tag{16}$$

For practical system implementation, we use the discrete-time dynamics of error-state:

$$\delta \boldsymbol{x}_N^{k+1} = \boldsymbol{\Phi}_k^{k+1} \delta \boldsymbol{x}_N^k + \boldsymbol{w}^k \tag{17}$$

where the index k denotes the k-th IMU measurement, and $\boldsymbol{w}^k$ is zero-mean white noise process with covariance $\boldsymbol{Q} := \mathrm{diag}(\boldsymbol{\sigma}_{v_a}^2, \boldsymbol{\sigma}_{v_g}^2, \boldsymbol{\sigma}_{\boldsymbol{\omega}_a}^2, \boldsymbol{\sigma}_{\boldsymbol{\omega}_g}^2)$, whose diagonal elements are covariances of $\boldsymbol{v}_a, \boldsymbol{v}_g, \boldsymbol{\omega}_a$, and $\boldsymbol{\omega}_g$. We use the Euler numerical integration method over the time interval δt between two IMU measurements to approximate the discrete-time error-state transition matrix as

$$\boldsymbol{\Phi}_k^{k+1} = \exp(\boldsymbol{F}(t_k)\delta t) \approx \boldsymbol{I}_{15} + \boldsymbol{F}(t_k)\delta t \tag{18}$$

And the discrete-time magnitude of the white noise sequence is derived as

$$\boldsymbol{Q}^k \approx \boldsymbol{G}(t_k)\boldsymbol{Q}\boldsymbol{G}(t_k)^\mathrm{T}\delta t \tag{19}$$

Thus, we obtain the covariance propagation equation as

$$\boldsymbol{P}_N^{k+1} = \boldsymbol{\Phi}_k^{k+1} \boldsymbol{P}_N^k \boldsymbol{\Phi}_k^{k+1\mathrm{T}} + \boldsymbol{Q}^k \tag{20}$$

3.2 UWB ranging measurement

There are various existing ranging schemes making use of UWB technology, such as TOF, TOA, and TDOA. Among these techniques, TOF was preferred in our work due to the fact that it is capable of

eliminating the need for anchor clock synchronization. Thus, unlike the work presented in Ref. [14], which determines both the anchor positions and clock offsets, we only need to localize the anchor positions during the deployment of UWB setup. For the UWB setup, the tag ranges with $m = 1, \ldots, M$ anchors in a round-robin scheme. A very precise clock is implemented in the UWB modules, thus an accurate transmission and reception time of the UWB signal was recorded. A double-sided Two Way Ranging (TWR) method[27] is used to measure the TOF. Figure 2 shows the core of a double-sided TWR exchange. The vertical lines represent time measurements by an anchor and tag, with their clocks independent and unsynchronized. It starts with a normal TWR exchange made up of a poll message and a response message. Upon receiving the response message, the tag sends a final message back to the anchor. The reply delays D_a and D_b are pre-defined constants; the round-trip times R_a and R_b are calculated by the measured message timestamps. Hence, the time of flight T_f is derived as

$$T_f = \frac{R_a R_b - D_a D_b}{R_a + D_a + R_b + D_b} \tag{21}$$

Once the TOF T_f is measured, the ranging measurement r^m between the tag and an anchor m is calculated and modeled as

$$r^m = T_f \cdot c = \|\boldsymbol{p}_m - \boldsymbol{p}^t\| + \boldsymbol{v}_r \tag{22}$$

where $\boldsymbol{p}_m$ is the position of the anchor m in the tangent frame, c the speed of radio wave, assumed to be equal to light speed, and $\boldsymbol{v}_r$ the ranging noise with a zero mean Gaussian distribution, $\boldsymbol{v}_r \sim \mathcal{N}(0, \sigma_{v_r}^2)$.

Finally, the Jacobians with respect to error terms $\delta\boldsymbol{p}_m$ and $\delta\boldsymbol{p}^t$ are needed for our self-localization solution. The Jacobian $\boldsymbol{J}_t$ with respect to $\delta\boldsymbol{p}^t$ at $\hat{\boldsymbol{p}}^t$ is straightforwardly obtained as

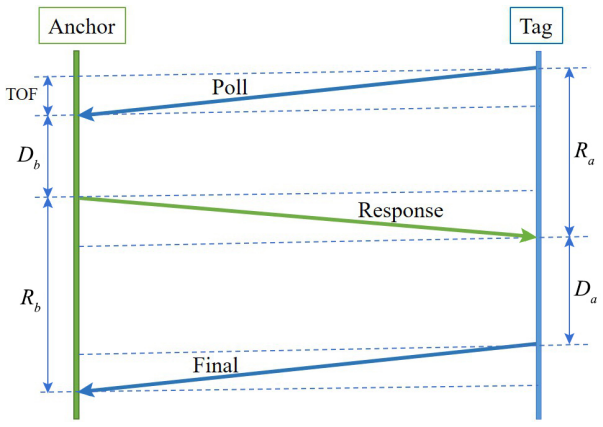

Fig. 2 A double-sided two-way ranging exchange.

$$\boldsymbol{J}_t = \frac{\partial\|\boldsymbol{p}_m - \boldsymbol{p}^t\|}{\partial\delta\boldsymbol{p}^t} = -\boldsymbol{e}^{\mathrm{T}} \tag{23}$$

$$\boldsymbol{e} = \frac{\boldsymbol{p}_m - \boldsymbol{p}^t}{\|\boldsymbol{p}_m - \boldsymbol{p}^t\|} \tag{24}$$

Here, $\boldsymbol{e}$ is the unit vector pointing from the anchor to the tag. The Jacobian $\boldsymbol{J}_m$ with respect to $\delta\boldsymbol{p}_m$ is

$$\boldsymbol{J}_m = \frac{\partial\|\boldsymbol{p}_m - \boldsymbol{p}^t\|}{\partial\delta\boldsymbol{p}_m} = \boldsymbol{e}^{\mathrm{T}} \tag{25}$$

4 Anchor Self-Localization Algorithm

In this section, we arrive at the solution to the anchor self-localization problem. The goal is to simultaneously estimate the positions of all unknown anchors and track the state of the tag. To derive a convergent and stable self-localization result, we need proper initialization.

4.1 Initialization

For proper initialization, the tag begins with a static state. Without loss of generality, the tangent frame origin is then set to be the position of the static tag, and the tangent frame axes coincide with the 3-dimensional accelerometer axes. We adopt a loosely-coupled fusion method to make initial guesses of the positions of anchors. Since the propagated positions of the tag by IMU measurements suffers little cumulative error for some time after system startup, accompanied by the UWB ranging measurements, we can calculate the initial values of the anchor positions using the multilateration equations.

Considering anchor m, we obtain the ranging measurements r_k^m and corresponding IMU propagated tag position $\boldsymbol{p}_k^t$ at timepoint k. Note that the UWB message contains the unique identity m of the communicating anchor. The initial anchor position $\boldsymbol{p}_{m,0}$ is then obtained by minimizing the objective function:

$$\boldsymbol{p}_{m,0} = \arg\min_{\boldsymbol{p}_m \in \mathbb{R}^3} \sum_{k=1}^{N} \|r_k^m - h(\boldsymbol{p}_m, \boldsymbol{p}_k^t)\| \tag{26}$$

where $h(\boldsymbol{p}_m, \boldsymbol{p}_k^t) = \|\boldsymbol{p}_m - \boldsymbol{p}_k^t\|$. Iterative Least-Squares (ILS) is utilized to solve this optimization. Note that, for a reliable initialization result, at least $N = 3$ UWB ranging measurements are needed while the tag is moving.

4.2 Tightly-coupled anchor self-localization

After initialization, we proceed with a tightly-coupled fusion of UWB ranging and inertial measurements for full state vector estimation. Figure 3 shows the proposed tightly-coupled fusion algorithm, where the

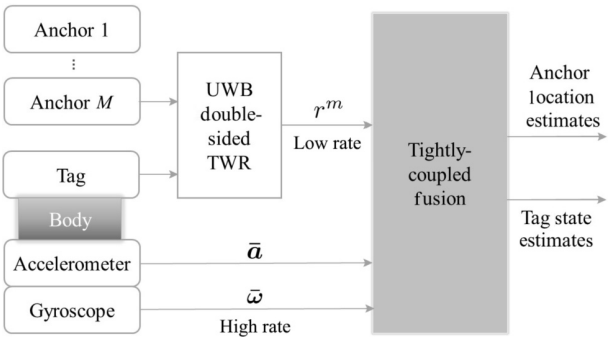

Fig. 3 Tightly-coupled fusion algorithm. Low rate UWB ranging measurements and high rate inertial measurements are directly used for simultaneous anchor self-localization and tag state estimation.

high-precision self-localization of anchors and the tracking of the tag are simultaneously performed. The low rate UWB ranging measurements and high rate inertial measurements are directly fed into the sensor fusion algorithm.

The fusion strategy is based on ESKF, which runs at the high rate of IMU to make full state predictions $\hat{\boldsymbol{x}}_S^-$ by IMU measurements and to propagate the error-state covariance matrix $\boldsymbol{P}$. At the arrival of low rate UWB measurement r^m emitting from the m-th anchor, which renders the errors observable, the filter correction is performed[28]:

$$\begin{aligned} \boldsymbol{K} &= \boldsymbol{P}\boldsymbol{H}^{\mathrm{T}}(\boldsymbol{H}\boldsymbol{P}\boldsymbol{H}^{\mathrm{T}} + \boldsymbol{\sigma}_{v_r}^2)^{-1}, \\ \delta\hat{\boldsymbol{x}}_S &= \boldsymbol{K}(r^m - h(\hat{\boldsymbol{x}}_S^-)), \\ \boldsymbol{P} &\leftarrow (\boldsymbol{I} - \boldsymbol{K}\boldsymbol{H})\boldsymbol{P} \end{aligned} \tag{27}$$

where $h(\hat{\boldsymbol{x}}_S^-) = h(\hat{\boldsymbol{p}}_m, \hat{\boldsymbol{p}}_k^t)$. The Jacobian matrix $\boldsymbol{H}$ with respect to the error-state $\delta\boldsymbol{x}_S$ is straightforwardly obtained as

$$\boldsymbol{H} = \left.\frac{\partial h}{\partial \delta \boldsymbol{x}_S}\right|_{\boldsymbol{x}_S} = \\ [\boldsymbol{J}_t \ \boldsymbol{0}_{1\times 12} \ \boldsymbol{0}_{1\times 3(m-1)} \ \boldsymbol{J}_m \ \boldsymbol{0}_{1\times 3(M-m)}] \tag{28}$$

By injecting the estimated error-state mean $\delta\hat{\boldsymbol{x}}_S$ into the prediction, the state estimate is updated using the appropriate compositions (quaternion products or sums):

$$\hat{\boldsymbol{x}}_S = \hat{\boldsymbol{x}}_S^- \oplus \hat{\delta\boldsymbol{x}}_S \tag{29}$$

5 Experimental Results

In this section we report on simulation experiments carried out to evaluate the performance of our proposed anchor self-localization method.

5.1 Simulation setup

In our simulation, the UWB setup is deployed in a large space, approximately 20 m × 20 m × 10 m in size. Five unsynchronized anchors are randomly placed at unknown locations. The inertial UWB tag has been mounted on an Unmanned Aerial Vehicle (UAV), which moves around the measurement volume for 30 seconds with high dynamics. The trajectory of the UAV follows a spiral pattern. Figure 4 shows the simulated ground truth of the anchor positions and the trajectory of the UAV.

The 50 Hz UWB ranging measurements and 100 Hz accelerometer and gyroscope measurements are then simulated using the ground truth with noise. As UWB ranging performs in a round-robin scheme, for each anchor the ranging measurement rate is 10 Hz which is relatively low. The UWB and IMU noise characteristics used for simulation are shown as follows: The standard deviation of the noise in the UWB ranging measurements is set as $\sigma_{v_r} = 0.01$ m, and the standard deviations of the white noise processes $\boldsymbol{v}_g, \boldsymbol{\omega}_g, \boldsymbol{v}_a$, and $\boldsymbol{\omega}_a$ in the IMU measurements are correspondingly set as $\boldsymbol{\sigma}_{v_g} = 6\times10^{-4}\cdot\boldsymbol{I}_3$ rad/s, $\boldsymbol{\sigma}_{\boldsymbol{\omega}_g} = 2\times10^{-4}\cdot\boldsymbol{I}_3$ rad/s^2, $\boldsymbol{\sigma}_{v_a} = 2\times10^{-3}\cdot\boldsymbol{I}_3$ m/s^2, and $\boldsymbol{\sigma}_{\boldsymbol{\omega}_a} = 8\times10^{-4}\cdot\boldsymbol{I}_3$ m/s^3, respectively.

The simulated measurements are fed into our method to simultaneously locate the anchors and track the states of the UAV. We evaluate the performance of our method in terms of the accuracy of the anchor self-localization and UAV state estimation.

5.2 Anchor self-localization results

Figure 5 shows the self-localization results of UWB anchors. The results are obtained from the last corrected state of ESKF and aligned with ground truth. We

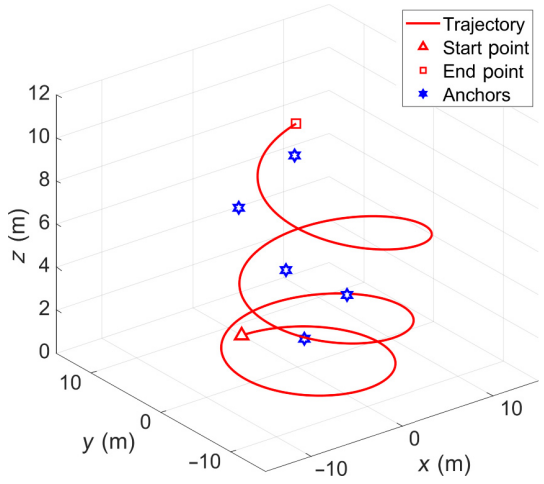

Fig. 4 Ground truth of positions of anchors and trajectory of the UAV. The red line is the simulated spiral trajectory and the blue six-pointed stars are positions of anchors.

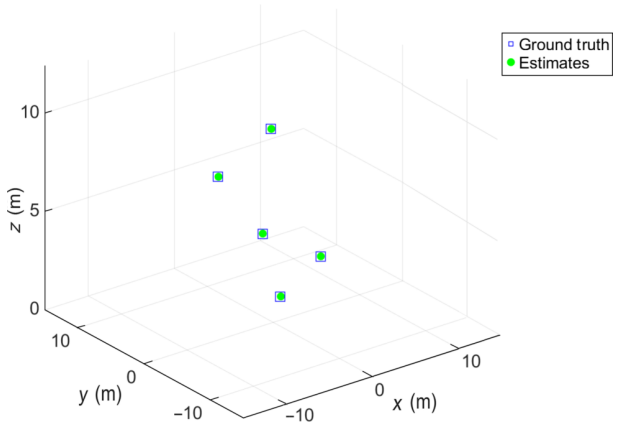

Fig. 5 Self-localization results of UWB anchors. The estimated anchor positions are depicted in green.

can see that the green dots indicating the results of our method are approximately superimposed over the blue indicating the ground truth. This suggests the effectiveness of our proposed self-localization method. The localization errors of each anchor are summarized in Table 1. The Root Mean Square Error (RMSE) for the anchors is 4.48 cm. The RMSE is given by

$$E_{\mathrm{RMSE}} = \sqrt{\frac{1}{N}\sum_{i=1}^{N}\|\boldsymbol{e}_i\|} \tag{30}$$

Figure 6 reflects the change of the anchor self-localization results over time. Without loss of

Table 1 Anchor self-localization errors. (cm)

	x	y	z
Anchor 1	5.60	2.78	0.17
Anchor 2	3.52	1.51	0.22
Anchor 3	0.09	0.38	0.88
Anchor 4	1.92	5.32	1.00
Anchor 5	2.90	1.92	0.70

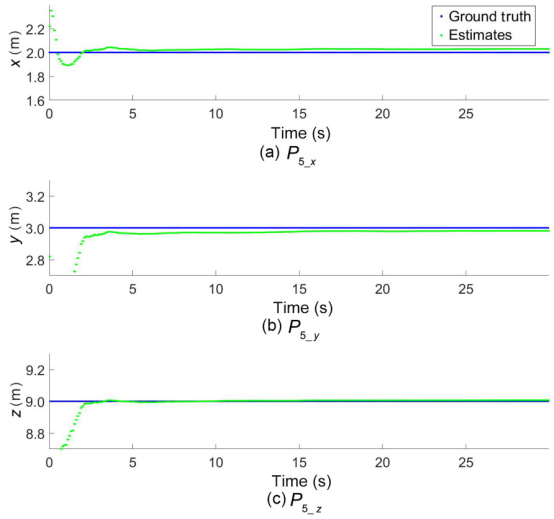

Fig. 6 Self-localization results of the 5-th anchor and its comparison against the ground truth.

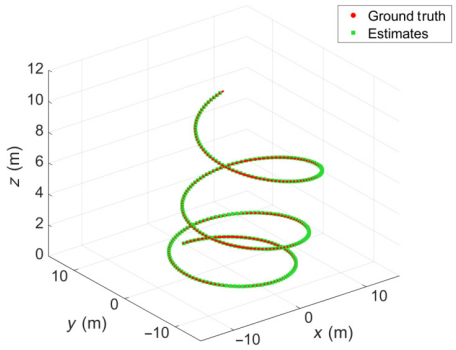

(a) Estimated trajectory and the ground truth

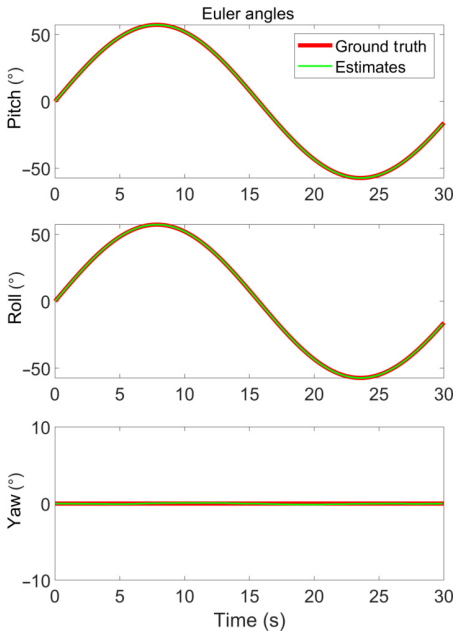

(b) Estimated orientation and the ground truth

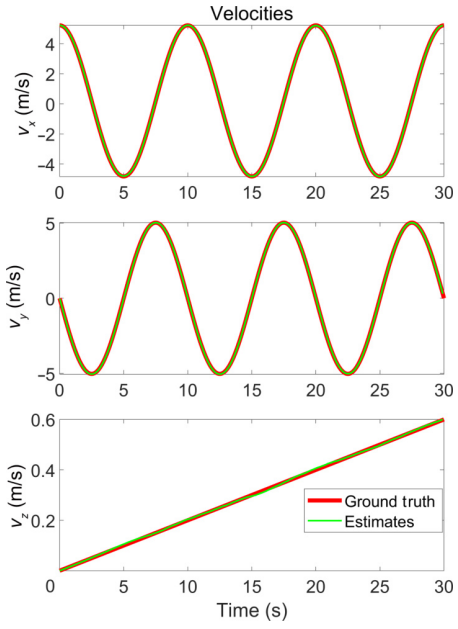

(c) Estimated speed and ground truth

Fig. 7 UAV state estimates and their comparison against the ground truth.

generality, we only show the results of the 5-th anchor. The results converge quickly and the errors in three coordinate axes remain low after approximately 5 seconds. Notably, a good initial guess of the anchor position by our initialization method aids in convergence.

5.3 Tag state estimation

Our method simultaneously localizes the anchors and estimates the UAV states. Figure 7 shows the state estimation results of our method and compares them against ground truth, wherein Fig. 7a shows the estimated UAV trajectory, Fig. 7b shows the estimated UAV orientation expressed by Euler angles, and Fig. 7c shows the estimated UAV speed. It can be seen that using our method the estimated positions of the UAV form a smooth trajectory, and that very smooth orientation and speed estimates are derived. From these results, we can conclude that our method enables accurate and smooth state estimates for the tag mounted UAV at the high output frequency. In support, the method achieves 5.59 cm RMSE for position and 0.1465° RMSE for orientation when comparing against the ground truth.

5.4 Performance under different ranging noise

To analyze the effect of ranging noise level on the performance of our method, we add varying noise on the UWB ranging measurements and evaluate the simulation results.

Figure 8 shows the results of the RMSE for anchor self-localization and tag positioning with respect to the ranging noise level. It can be seen that the RMSE grows approximately linearly as ranging noise increases.

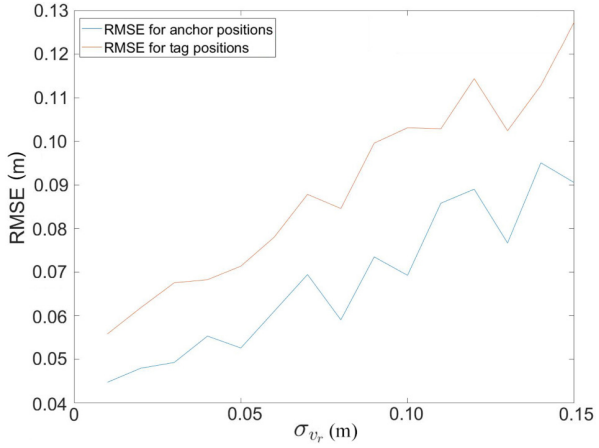

Fig. 8 Performance of our method with respect to UWB ranging noise.

Though the covariance of the ranging measurements reached 0.15, a satisfying result can be obtained with 0.0905 m RMSE for anchors and 0.1273 m RMSE for the tag. This indicates the robustness of our method.

6 Conclusion

In this work, we have presented an accurate and easy-to-use UWB anchor self-localization method, using the UWB TOF measurements and inertial measurements. Inspired by the SLAM technique, our method simultaneously localizes the UWB anchor and estimates the state of the moving tag, thus enabling automatic deployment of UWB setup while freely moving the tag in the environment. Experiments show that the method permits accurate and robust UWB anchor self-localization within a few seconds, and is capable of drift-free localization of the moving tag.

References

[1] H. Liu, H. Darabi, P. Banerjee, and J. Liu, Survey of wireless indoor positioning techniques and systems, *IEEE Trans. Syst., Man, Cybern. C: Appl. Rev.*, vol. 37, no. 6, pp. 1067–1080, 2007.

[2] S. Gezici, Z. Tian, G. B. Giannakis, H. Kobayashi, A. F. Molisch, H. V. Poor, and Z. Sahinoglu, Localization via ultra-wideband radios: A look at positioning aspects for future sensor networks, *IEEE Signal Proc. Mag.*, vol. 22, no. 4, pp. 70–84, 2005.

[3] L. Zwirello, M. Janson, C. Ascher, U. Schwesinger, G. F. Trommer, and T. Zwick, Localization in industrial halls via ultra-wideband signals, in *Proc. 2010 7^{th} Workshop on Positioning, Navigation and Communication*, Dresden, Germany, 2010, pp. 144–149.

[4] Y. Q. Qin, F. Wang, and C. J. Zhou, A distributed UWB-based localization system in underground mines, *J. Net.*, vol. 10, no. 3, pp. 134–140, 2015.

[5] T. M. Nguyen, A. H. Zaini, K. X. Guo, and L. H. Xie, An ultra-wideband-based multi-UAV localization system in GPS-denied environments, in *Int. Micro Air Vehicle Conf. Competition*, Beijing, China, 2016.

[6] R. Bharadwaj, S. Swaisaenyakorn, C. G. Parini, J. C. Batchelor, and A. Alomainy, Impulse radio ultra-wideband communications for localization and tracking of human body and limbs movement for healthcare applications, *IEEE Trans. Anten. Propag.*, vol. 65, no. 12, pp. 7298–7309, 2017.

[7] K. X. Guo, Z. R. Qiu, C. X. Miao, A. H. Zaini, C. L. Chen, W. Meng, and L. H. Xie, Ultra-wideband-based localization for quadcopter navigation, *Unmanned Syst.*, vol. 4, no. 1, pp. 23–34, 2016.

[8] I. Guvenc, C. C. Chong, and F. Watanabe, Joint TOA estimation and localization technique for UWB sensor network applications, in *Proc. 2007 IEEE 65^{th} Vehicular*

Technology Conf. VTC2007-Spring, Dublin, Ireland, 2007, pp. 1574–1578.

[9] C. Zhang, M. Kuhn, B. Merkl, A. E. Fathy, and M. Mahfouz, Accurate UWB indoor localization system utilizing time difference of arrival approach, in *Proc. 2006 IEEE Radio and Wireless Symp.*, San Diego, CA, USA, 2006, pp. 515–518.

[10] J. Xu, M. D. Ma, and C. L. Law, Position estimation using UWB TDOA measurements, in *Proc. 2006 IEEE Int. Conf. Ultra-WideBand* (*ICUWB*), Waltham, MA, USA, 2006, pp. 605–610.

[11] J. Tiemann, F. Schweikowski, and C. Wietfeld, Design of an UWB indoor-positioning system for UAV navigation in GNSS-denied environments, in *Proc. 2015 Int. Conf. Indoor Positioning Indoor Navigation* (*IPIN*), Banff, Canada, 2015, pp. 1–7.

[12] J. Wang, R. K. Ghosh, and S. K. Das, A survey on sensor localization, *J. Control Theory Appl.*, vol. 8, no. 1, pp. 2–11, 2010.

[13] J. D. Hol, T. B. Schön, and F. Gustafsson, Ultra-wideband calibration for indoor positioning, in *Proc. 2010 IEEE Int. Conf. Ultra-WideBand* (*ICUWB*), Nanjing, China, 2010, pp. 1–4.

[14] M. Kok, J. D. Hol, and T. B. Schön, Indoor positioning using ultrawideband and inertial measurements, *IEEE Trans. Veh. Technol.*, vol. 64, no. 4, pp. 1293–1303, 2015.

[15] D. M. Henderson, Euler angles, quaternions, and transformation matrices for space shuttle analysis, https://ntrs.nasa.gov/search.jsp?R=19770019231, 1977.

[16] M. W. M. G. Dissanayake, P. Newman, S. Clark, H. F. Durrant-Whyte, and M. Csorba, A solution to the simultaneous localization and map building (SLAM) problem, *IEEE Trans. Rob. Autom.*, vol. 17, no. 3, pp. 229–241, 2001.

[17] H. Durrant-Whyte and T. Bailey, Simultaneous localization and mapping: Part I, *IEEE Robot. Autom. Mag.*, vol. 13, no. 2, pp. 99–110, 2006.

[18] T. Bailey and H. Durrant-Whyte, Simultaneous localization and mapping: Part II, *IEEE Robot. Autom. Mag.*, vol. 13, no. 3, pp. 108–117, 2006.

[19] C. Cadena, L. Carlone, H. Carrillo, Y. Latif, D. Scaramuzza, J. Neira, I. Reid, and J. J. Leonard, Past, present, and future of simultaneous localization and mapping: Toward the robust-perception age, *IEEE Trans. Robot.*, vol. 32, no. 6, pp. 1309–1332, 2016.

[20] R. Smith, M. Self, and P. Cheeseman, A stochastic map for uncertain spatial relationships, in *Proc. 4^{th} Int. Symp. Robotics Research*, Santa Clara, CA, USA, 1987, pp. 467–474.

[21] J. Solà, Simulataneous localization and mapping with the extended Kalman filter, http://www.iri.upc.edu/people/jsola/JoanSola/objectes/curs_SLAM/SLAM2D/SLAM%20course.pdf, 2013.

[22] J. D. Hol, F. Dijkstra, H. Luinge, and T. B. Schön, Tightly coupled UWB/IMU pose estimation, in *Proc. 2009 IEEE Int. Conf. Ultra-Wideband* (*ICUWB*), Vancouver, Canada, 2009, pp. 688–692.

[23] L. Zwirello, X. Y. Li, T. Zwick, C. Ascher, S. Werling, and G. F. Trommer, Sensor data fusion in UWB-supported inertial navigation systems for indoor navigation, in *2013 IEEE Int. Conf. Robotics and Automation*, Karlsruhe, Germany, 2013, pp. 3154–3159.

[24] M. W. Mueller, M. Hamer, and R. D'Andrea, Fusing ultra-wideband range measurements with accelerometers and rate gyroscopes for quadrocopter state estimation, in *2015 IEEE Int. Conf. Robotics and Automation* (*ICRA*), Seattle, WA, USA, 2015, pp. 1730–1736.

[25] P. S. Maybeck and G. M. Siouris, Stochastic models, estimation, and control, *IEEE Trans. Syst. Man Cybern.*, vol. 10, no. 5, p. 282, 1980.

[26] J. A. Farrell, *Aided Navigation*: *GPS with High Rate Sensors*. New York, NY, USA: McGraw-Hill, 2008, pp. 354–377.

[27] D. Neirynck, E. Luk, and M. McLaughlin, An alternative double-sided two-way ranging method, in *2016 13^{th} Workshop on Positioning, Navigation and Communicatins* (*WPNC*), Bremen, Germany, 2016, pp. 1–4.

[28] J. Solà, Quaternion kinematics for the error-state Kalman filter, arXiv preprint arXiv: 1711.02508, 2017.

Xiaowei Cui is an associate professor in the Department of Electronic Engineering, Tsinghua University, China. He obtained the BS and PhD degrees in electronic engineering from Tsinghua University in 1999 and 2004, respectively. He is a member of the Expert Group of China BeiDou Navigation Satellite System. His research interests include robust GNSS signal processing, multipath mitigation techniques, and high-precision positioning.

Qin Shi is a PhD candidate in the Department of Electronic Engineering at Tsinghua University, China. He received the BS degree from Tsinghua University in 2015. His current research focuses on indoor localization, sensor fusion, and simultaneous localization and mapping.

Sihao Zhao is a lecturer in the Department of Electronic Engineering, Tsinghua University. He received the BS and PhD degrees from Tsinghua University in 2005 and 2011, respectively. His research interests include GNSS signal processing algorithms, high-precision positioning techniques, indoor navigation systems as well as telecommunication systems design and verification.

Mengdi Jia is an assistant engineer in Beijing Electric Power Company of State Grid Corporation of China. She received the MS degree from Tsinghua University, China in 2017. Her research interests include INS and integrated navigation.

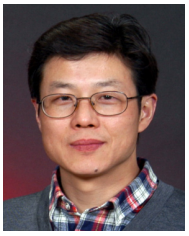

Mingquan Lu is a professor of the Department of Electronic Engineering, Tsinghua University, China. He is the director of Tsinghua Position, Navigation and Timing Center, and a member of the Expert Group of China BeiDou Navigation Satellite System. His current research interests include GNSS signal design and analysis, GNSS signal processing and receiver development, and GNSS system modeling and simulation. He received the MS and PhD degrees from University of Electronic Science and Technology of China in 1993 and 1999, respectively.